Journal of Bio- and Tribo-Corrosion (2020) 6:49
https://doi.org/10.1007/s40735-020-00346-x

Electroplating of Nanocrystalline Ni–Co Alloys Using Cysteine and Their Electrochemical Behaviour in NaOH Solution

Mosaad Negem[1,2] · N. Helal[2] · S. Roy[1] · H. Elfeky[2] · G. Kardas[3]

Received: 9 January 2020 / Revised: 15 February 2020 / Accepted: 4 March 2020 / Published online: 11 March 2020

Abstract
Electroplated Ni–Co alloys show superior electrocatalytic activity towards hydrogen evolution reaction. In this work, the cysteine and sodium gluconate obtained from natural products were utilized to electroplate the nanocrystalline Ni–Co alloys. The electroplating baths were characterized using cathodic polarization technique. The effect of sodium gluconate, cysteine and boric acid on the surface morphology of the electroplated Ni–Co alloys was studied using scanning electron microscopy (SEM). Chemical composition of the electroplated Ni–Co alloys was determined using the energy dispersive X-ray (EDX), and their crystal lattice system was examined by X-ray diffraction (XRD) analysis. The X-ray diffraction pattern confirms that the electroplated Ni–Co alloys with Co% of 1–75% arranged in face-centred cubic (FCC) structure, while the electroplated Ni–Co alloys with Co% more 76% positioned in hexagonal closed-package (HCP) structure. The thickness of the Ni–Co alloys varied between 14.61 and 27.94 µm. The cathodic polarization data show that gluconate and cysteine enhance electroplating of Ni–Co alloys by decreasing the overpotential of Ni^{2+} and Co^{2+} reduction reaction. Potentiodynamic polarization was utilized to study the electrochemical behaviour of the Ni–Co alloys in NaOH aqueous solutions, which indicated that electroplated Ni–Co alloys with low Co% displayed the low rate of corrosion.

Keywords Ni–Co alloys · Cathodic polarization · Nanocrystalline · Potentiodynamic polarization

1 Introduction

Electroplating of metals and alloys has great interests for various applications. Electroplated Ni alloys possess high electrocatalytic activity, superior mechanical properties, corrosion resistance, thermo-physical and magnetic properties [1–3]. Nanocrystalline Ni alloys have been used as cathodes for the hydrogen evolution reaction [4–8]. In addition, Ni alloys are characterized by the high hardness and the superior corrosion resistance, which is likely to be substituted for hard alloys such as hard chromium materials [9]. Moreover, nickel alloys have good resistance to corrosion under atmospheric, aqueous neutral pH and deaerated non-oxidizing acidic medium. In addition, Ni–Co alloys show superior resistance to corrosion in caustic alkalis [10, 11] and can be utilized as cathodes for hydrogen evolution reaction.

Electroplated Ni alloys can be greatly influenced by different chemical additives which can produce a dense thin film for corrosion protection of different substrates in alkaline solution. The effect of different additives such as gluconate, boric acid, and cysteine on the electroplating of Ni–Co alloys is investigated during this study. Additives such as complexing agent, brighteners and antipitter can improve to a great extent the mechanical and surface morphology of the electroplated Ni–Co alloys. Electroplating of Ni–Co alloys was performed using the organic refiner such as saccharin which led to the formation of nanocrystalline structures [12]. Most hard Ni coatings produced using the electroplating technique had high tensile intrinsic stress [13]. Addition of straight-chain organic sulphur compounds decreases the stress and produces dense and smooth coatings. The natural mercapto compounds such as cysteine produce bright and fine granular coatings. The present work studies the electroplating of Ni–Co alloys using gluconate-cysteine bath under the galvanostatic condition and investigates the electrochemical behaviour of the

✉ Mosaad Negem
mra00@fayoum.edu.eg

[1] School of Chemical Engineering and Advanced Materials, Newcastle University, Newcastle upon Tyne NE1 7RU, UK

[2] Chemistry Department, Faculty of Science, Fayoum University, Fayoum 63514, Egypt

[3] Department of Chemistry, Cukurova University, Adana, Turkey

electroplated Ni–Co alloys in sodium hydroxide solutions using potentiodynamic polarization.

2 Experimental Methods

Cathodic polarization measurements were performed using μAutolab system II, operated by GPES software with a scan rate of 5 mV/s from the open circuit potential. Moreover, the potential was started from open circuit potential (OCP) of approximately − 0.25 V moving to the more negative potential of − 2.0 V. The cell was a three-electrode all-glass cell, with a platinum counter electrode of dimensions 10 mm × 5 mm × 0.2 mm, and saturated calomel electrode was used as a reference electrode. Similarly, the electrochemical behaviour of Ni, Co and Ni–Co alloys was also investigated using the μAutolab system II with a scan rate of 10 mV/s, starting at 0 V and moved to anodic direction then it reversed to the cathodic direction. In addition, TTi Thurlby Thandar instrument PL310 (32 V-1A) PSU was used as the source of the direct current. Copper foils with a purity of 99.98% were utilized as a cathode (substrate), and a platinum mesh was the anode. The plating cell was a Pyrex cylinder of volume (1.2 L) with PTFE lid which contained five holes; these holes were utilized to insert the electrodes and thermometer.

Chemicals of Aldrich-Sigma grade were utilized in the electroplating baths such as $NiSO_4 \cdot 7H_2O$, $CoSO_4 \cdot 7H_2O$, H_3BO_3, sodium gluconate and cysteine. The chemicals were weighed and dissolved in deionized water, as shown in Table 1. The different concentrations of the chemicals were operated to optimize the electroplating of Ni–Co alloys. Also, sodium hydroxide (Aldrich grade) was utilized to study the electrochemical behaviour of Ni, Co and Ni–Co alloys.

The electroplating experiments of Ni, Co and Ni–Co alloys were performed via stagnant gluconate baths using a constant current density varied between 0.1 and 5 Adm^{-2}. The electroplating time was one hour at 293 K on copper sheet. To stabilize the concentration of bath species, a fresh bath was prepared. Before each run, the copper substrate was etched in concentrated nitric acid (1:1) for 1 min to remove the oxides layer, then washed with deionized water, rinsed with acetone and weighed. The cathodic current efficiency was determined by weight measurement before and after the electroplating process. Electrochemical behaviour of the obtained Ni, Co and Ni–Co alloys was studied using potentiodynamic polarization in stagnant, naturally aerated sodium hydroxide solutions (0.01, 0.1, 1.0 M). Before each experiment, the working electrode was about 0.2 cm^2 surface area to contact the solution. This working electrode was immersed quickly into the sodium hydroxide solution.

The surface morphology of the electroplated Ni, Co and Ni–Co alloys was examined by scanning electron microscopy (SEM) (JEOL JSM-5300 LV, at 25 kV under high vacuum). Furthermore, the chemical composition of the electroplated Ni–Co alloys was determined by energy dispersive X-ray analysis. The nanostructure of the Ni, Co and Ni–Co alloys was determined by X-ray diffraction with Philips X'Pert Pro Diffractometer, fitted with the X'Celerator and a secondary monochromator. To generate copper K-alpha radiation with a wavelength of 1.54 Å, a copper anode was supplied with a voltage of 40 kV and current of 0.04 A. The thickness of the electroplated Ni–Co alloys was determined using an optical microscope (OLYMPUS BX41 with Soft Imaging System).

3 Results and Discussion

3.1 Bath Characterization

Figure 1 illustrates the cathodic polarization curves performed using different electrolytes of Ni^{2+} or Co^{2+} and mixture of Ni^{2+} and Co^{2+} without and with different additives. The cathodic polarization curves displayed three growth region of cathodic current density which were a, b

Table 1 Baths were utilized to electrodeposit nickel, cobalt and their alloys using current density of 0.4 Adm^{-2} at 293 K

Bath	$NiSO_4$ (M)	$CoSO_4$ (M)	Sodium gluconate (M)	H_3BO_3 (g/l)	Cysteine (M)	pH
1	0.100	–	–	–	–	5.79
2	0.100	–	0.1	–	–	5.81
3	0.100	–	0.1	10	–	3.99
4	0.100		0.1	10	0.018	4.00
5	0.090	0.01	0.1	10	0.018	4.00
6	0.085	0.015	0.1	10	0.018	4.02
7	0.075	0.025	0.1	10	0.018	4.03
8	0.070	0.030	0.1	10	0.018	4.05
9	0.050	0.050	0.1	10	0.018	4.07
10	0.030	0.070	0.1	10	0.018	4.08
11	–	0.100	0.1	10	0.018	4.10

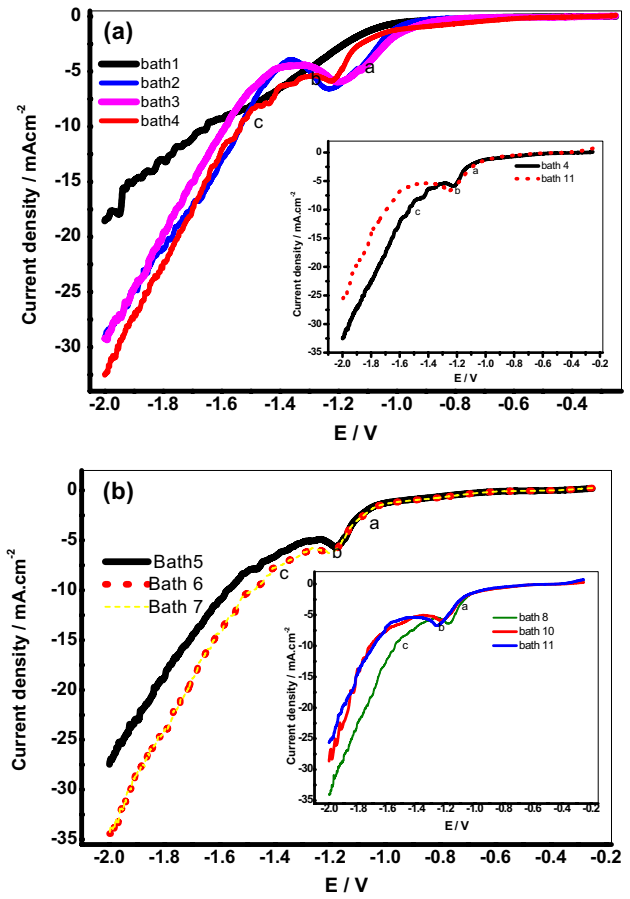

Fig. 1 Cathodic polarization curves of the electroplating baths for Ni–Co alloys with scan rate 5 m V/s at 293 K; **a** Baths 1, 2, 3 and 4; **b** baths 5, 6, 7, 8, 10 and 11

and c. During region a, reduction of Ni^{2+} to Ni^{+} occurred, this was proved by many researchers [3, 14]. In the region b, the reduction of Ni^{+} to Ni occurs and region c includes the hydrogen evolution reaction. The additives have a great effect on the reduction potential. Gluconate (baths 2) shifted significantly reduction potential of Ni^{2+} (regions a and b) to less negative values than Ni^{2+} (bath 1) which possesses very small reduction region, begun at − 0.9 V. Addition of boric acid as in bath 3 slightly moved the reduction potential of Ni than bath 2, to more positive value. Besides, the addition of cysteine (bath 4) shifted the reduction potential of Ni^{2+} to more positive values than that obtained by bath 1.

The electroplating potential of Ni^{2+} and Co^{2+} bath shifted gradually to a more positive value of − 1.175 V than that obtained using bath 1 as shown in Fig. 1b for baths 5, 6, 7 and 8. However, the shift of electroplating potential for the baths 10 and 11 was slightly moved to a more negative value of about − 1.19 V than bath 8. Comparing the cathodic polarization curve of the bath 4 of Ni^{2+} and bath 11 of Co^{2+}, the electroplating potential of Ni^{2+} was slightly more positive than Co^{2+}. Besides, region c shifted at potential about − 1.5 V which included sharply growth of cathodic current density due to reduction of H^{+}.

The more positive shift of the reduction potential of Ni^{2+} and Co^{2+} due to the presence of the additives can be explained by the promotion of the initiation of Ni nucleation and delaying of the hydrogen reduction. The findings indicate that the addition of agents can effectively change and improve the microstructure and properties of the electroplated Ni–Co alloys. Sodium gluconate in the electroplating bath may act as a ligand for nickel ions leading to change in the film from burnt to white. These results are due to the formation of Ni–gluconate complex, which accelerates the transfer of electrons via ion bridging [3, 14] and which increases the rate of electroplating as can be seen from cathodic polarization measurements and lower the overpotential of Ni reduction reaction. Hydrogen evolution causes the formation of pits in coatings, but they were improved to less porous and granular grains by adding boric acid (anti-pitters). In fact, this effect could be due to the adsorption of boric acid species at the cathode which can minimize the effective surface available for proton reduction [15] and it is indicated by showing the more positive shift of electroplating potential of Ni or which enhance the reduction rate. The adsorption of Ni-boric acid complex species on the cathode may also lower the overpotential which is necessary for electroplating of Ni in sulphate solutions [16]. Therefore, boric acid increases the nucleation rate of Ni and Co as can be seen in Fig. 1.

Bright electrodeposited Ni–Co alloys were obtained by adding a brightening agent such as cysteine. The effect of cysteine can be attributed to its adsorption at the cathode surface; the adsorption of cysteine molecules at metal electrodes is related to the interaction of lone pair of electrons of –SH, –COOH and $–NH_2$ groups with the Ni and Co ions and electrode surface as a ligand [14]. Cysteine follows non-blocking adsorption which occurs on the active sites of the crystal planes of the substrates and on the emerging surfaces of the crystallizing phases [17]. Therefore, cysteine can act as a hindrance and decelerate surface diffusion of adsorbed ions [18]. This causes more difficult grain growth and consequently higher nucleation rate, resulting in finer grains. Also, cysteine can form a complex with metal ions, increasing the number of formed complexes adsorbed on the electrode, and thus increase the rate of reduction (induced adsorption) or accelerating the rate of flow of electrons through the additive from the electrode to the metal ion (ion bridging) [3]. Cysteine supports similarly the electroplating of Ni and Co and due to shift of reduction potential to a more positive direction and small overpotential.

3.2 Morphology, Composition and Crystal Lattice of the Electroplated Ni–Co Alloys

Figure 2 shows the SEM images of electroplated Ni, Co and Ni–Co alloys obtained using a current density of 0.4

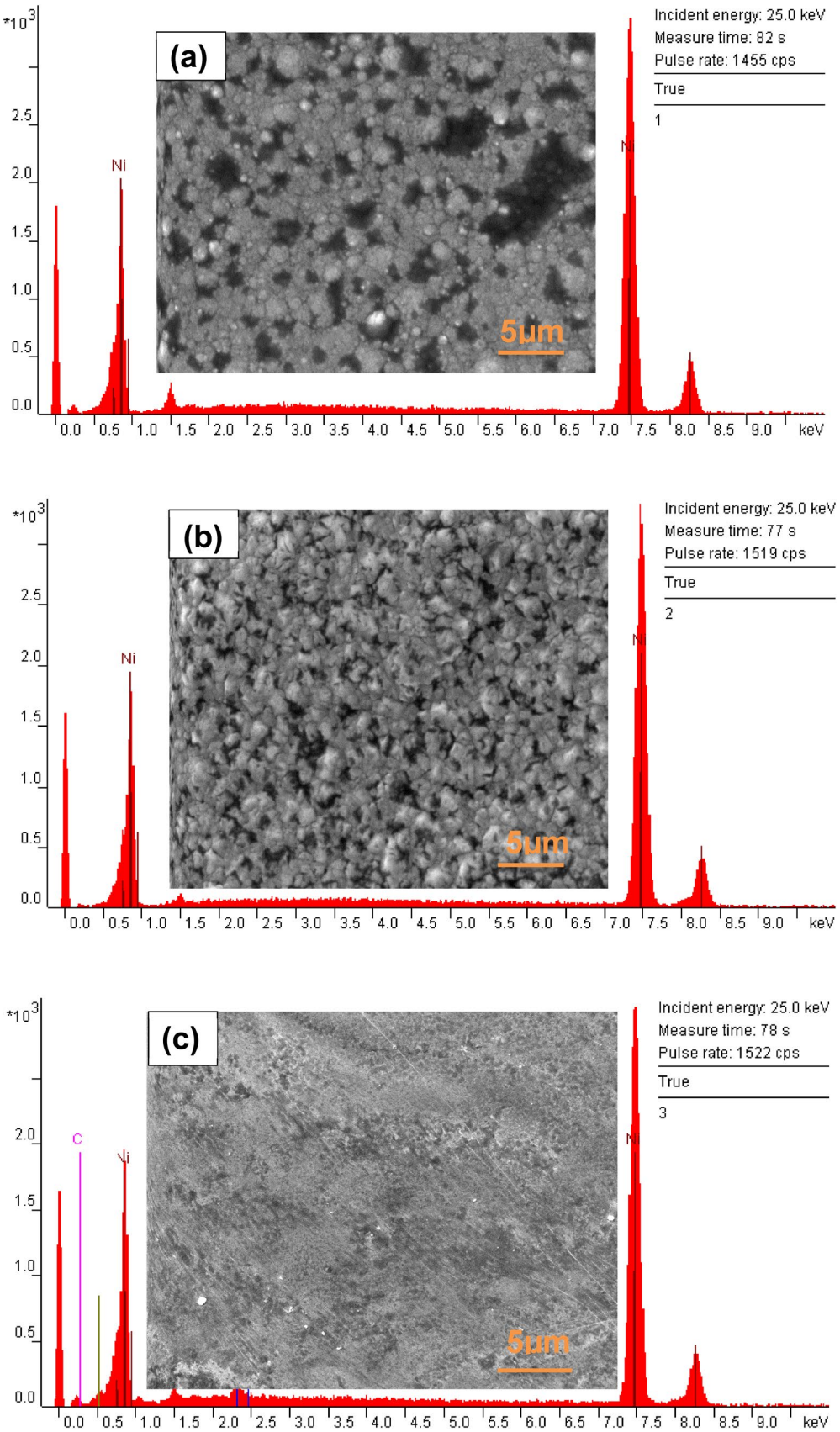

Fig. 2 SEM images of the electroplated Ni, Co and Ni–Co alloys obtained using gluconate bath, **a** Ni (bath 2), **b** Ni (bath 3), **c** Ni (bath 4), **d** Ni-92.05Co **e** Ni-97.36Co, **f** cobalt (99.76%)

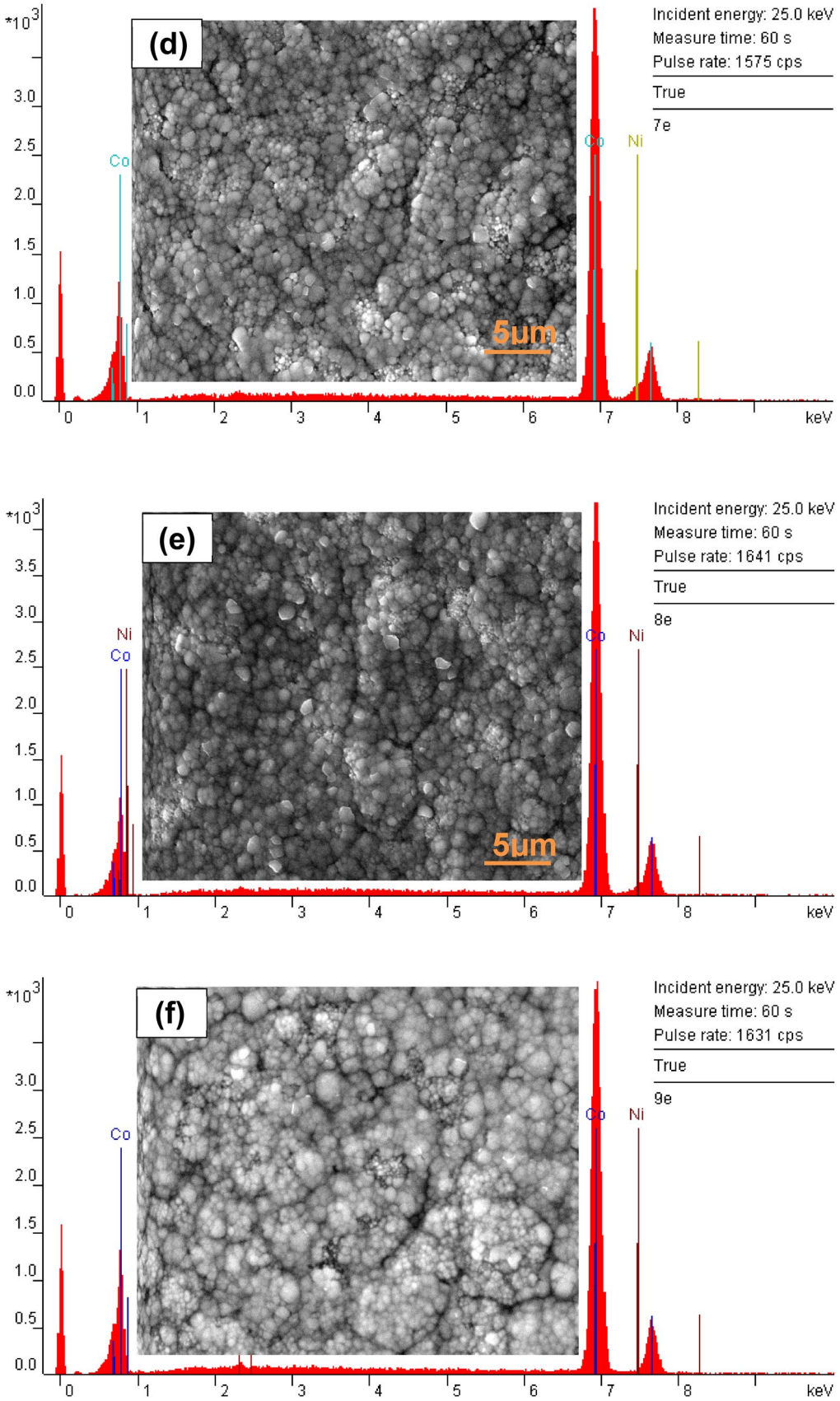

Fig. 2 (continued)

Adm^{-2} for 1 h at 293 K. The surface morphology of Ni was changed from burnt and porous to dense and shiny as shown in Fig. 2a–c. The additives included organic additives of sodium gluconate and cysteine and an inorganic additive of boric acid. The electroplated Ni obtained using bath 1 was burnt and porous. The slightly porous and granular Ni was obtained by addition of gluconate to the bath. Moreover, boric acid removes effectively pinholes, creates a granular coating. The presence of cysteine in the bath created dense and shiny Ni, as displayed in Fig. 2c. The surface morphology was dense for the Ni–Co alloys that contained a range of Co content between 1 and 45% such as Ni, Ni-17.68Co, Ni-34.81Co and Ni-42.44Co, as can be seen in Fig. 2c. However, with the rise of Co content in the Ni–Co alloys more than 45%, the micrograph revealed the spherical and nodular or coral reef-like structure of Ni-60.21Co, Ni-74.46Co, Ni-92.05Co alloys and Co, as can be seen in Fig. 2d–f. EDX analysis showed that electroplated Ni–Co alloys of different Co% were obtained from gluconate baths such as Ni-17.68Co, Ni-34.81Co, Ni-42.44Co, Ni-60.21Co, Ni-74.46Co Ni-92.05Co and Ni-97.36Co, as merged in Fig. 2 and Table 2.

Figure 3 displays XRD patterns of the electroplated Ni–Co alloys which displayed intensity peaks relating to nanocrystalline structures. The XRD patterns assured that Ni–Co alloys with Co % of 1–75% assembled in face-centred cubic (JCPDS number 35-1360) with unit cell parameters increase from $a = 3.681$ Å to $a = 3.69$ Å. Besides, the Ni–Co alloys with Co% more than 75% organized in hexagonal closed package HCP(JCPDS number 05-0727). The electroplated Ni, Ni-17.68Co, Ni-34.81Co, Ni-42.44Co, Ni-60.21Co, Ni-74.46Co alloys arranged in FCC lattice which possess lower interfacial free energy than HCP structures.

Table 2 Chemical compositions obtained from EDX analysis of coatings Ni, Co and Ni–Co alloys obtained using gluconate bath and a direct current of 0.4 Adm^{-2} at 293 K

Bath	Ni%	Co%
4	99.8	–
5	80.7	17.68
6	62.9	34.81
7	55.3	42.44
8	37.8	60.21
9	25.54	74.46
10	7.95	92.05
11	–	99.7

Nonetheless, electroplated Ni-92.05Co and Co98.76% form HCP structures. Moreover, Nickel and cobalt are chemically and physically similar elements; because of the typical atomic size. Therefore, the electroplating of Ni and Co completely produces homogeneous alloys as a substitution solid solution [19]. The average grain size of the electroplated Ni–Co alloys coatings was calculated using Debye–Scherrer's equation [20]: $\tau = (K\lambda)/(\beta \cos\theta)$ where λ is the X-ray wavelength, typically 1.54 Å, β is the line broadening at half the maximum intensity in radians, K is the shape factor, θ is the Bragg angle and τ is the mean size of the ordered (crystalline) domains. The average grain size of Ni–Co alloys with Co% of 0–75% varied between 6.5 and 16.6 nm, while the average grain size of Ni–Co alloys with Co% of more than 75% varied between 20 and 22 nm.

Figure 4 shows the current efficiency of the electroplated Ni, Co and Ni–Co alloys which increased gradually with the increase of cobalt content. The lowest value of cathodic current efficiency was for Ni at nearly 66%. Moreover, the Ni-17.68Co, Ni-60.21Co, Ni-74.46Co and Ni-92.05Co alloys displayed the gradual increase of cathodic current efficiency of 71%, 72%, 73.9% and 75%, respectively. The highest current efficiency was obtained for pure Co, which was calculated about 75.8%. The thickness of coatings increased gradually with the increase of Co content in the alloys. The smallest thickness was obtained for Ni which is 14.61 µm. It was followed by Ni-17.68Co, Ni-60.21Co and Ni-74.46Co alloys, which were 17.71 µm, 26.19 µm, 27.94 µm and 27.72 µm, respectively, as shown in Fig. 4.

3.3 Potentiodynamic Polarization

Corrosion data were obtained using the potentiodynamic polarization curves as shown in Fig. 5 for electroplated Ni–Co alloys immersed in different concentrations of sodium hydroxide solution (0.01 M, 0.1 M and 1.0 M) at 293 K. The corrosion parameters were calculated using the Tafel extrapolation such as corrosion current density (i_{corr}), corrosion potential (E_{corr}), anodic Tafel slopes (β_a) and (β_c), as displayed in Table 3. The Electroplated Ni–Co alloys with high Ni% displayed low i_{corr} but i_{corr} is increased for Ni–Co alloys with high Co%. The electroplated Ni-17.68Co alloy possesses the lower i_{corr} of 0.08 µA/cm^2 in 0.01 M sodium hydroxide. However, the Ni-92.05Co alloy shows higher i_{corr} of 3.5 µA/cm^2 in 0.01 M NaOH solution. The i_{corr} of the electroplated Ni–Co alloys increases with the increase

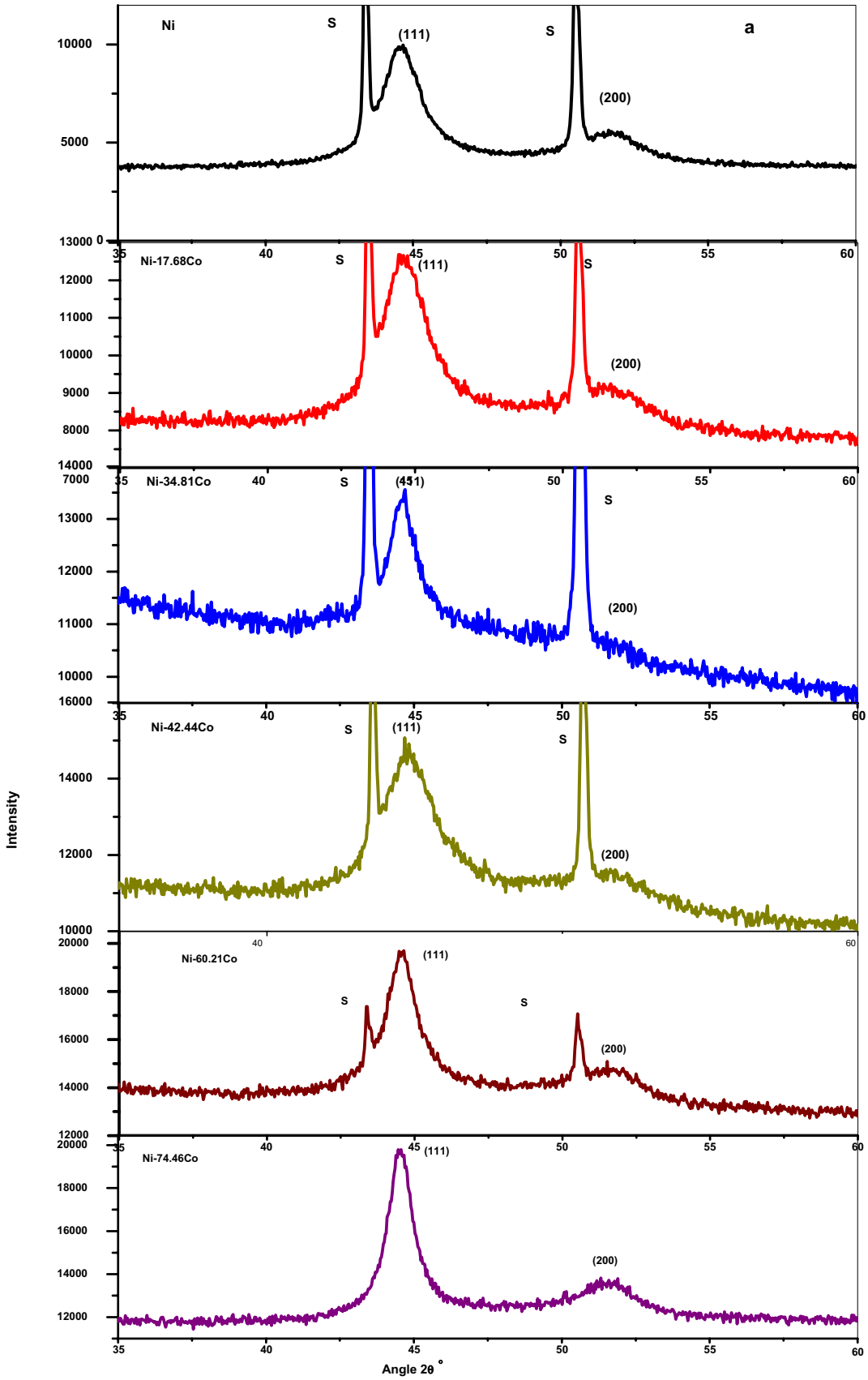

Fig. 3 XRD patterns of electroplated Ni, Co and their alloys from gluconate bath using 0.4 A dm^{-2} for 1 h at 293 K, where **a** Ni, Ni-17.68Co, Ni-34.81Co, Ni-42.44Co, Ni-60.21Co and Ni-74.46Co of FCC structures, **b** Ni-92.05Co and Co of HCP structures

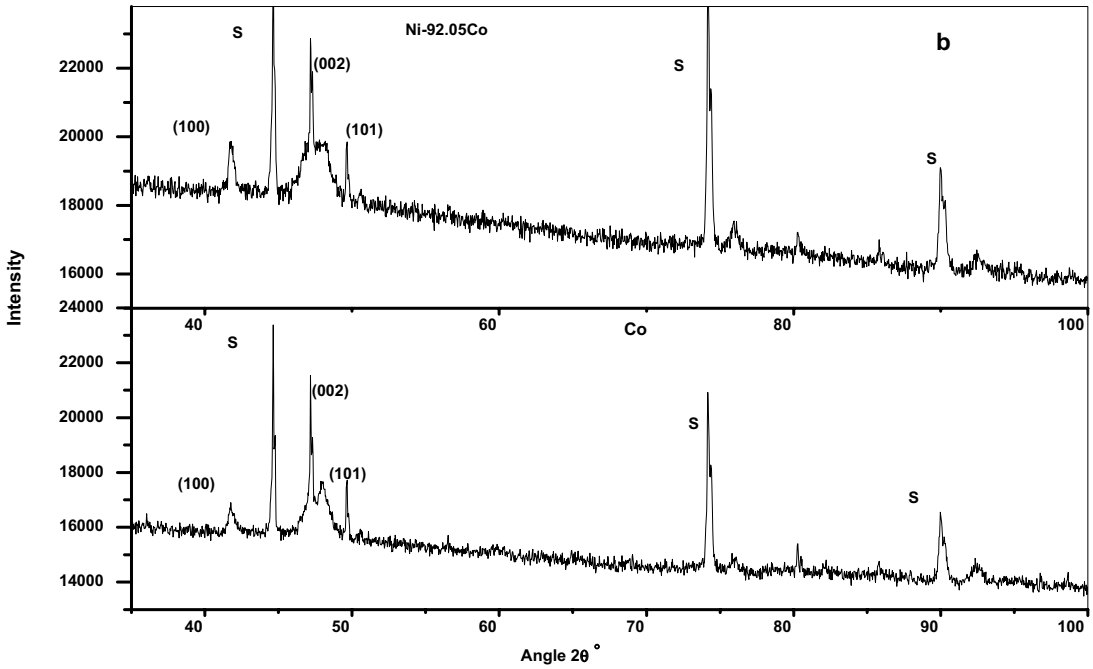

Fig. 3 (continued)

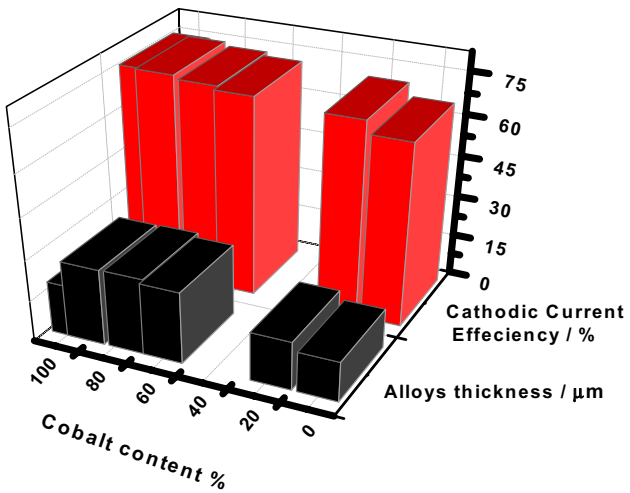

Fig. 4 The variation of the cathodic current efficiency and thickness of electroplated Ni, Co and Ni–Co alloys with Co%

of sodium hydroxide concentrations. The mixed corrosion potential, E_{corr}, for the electroplated Ni–Co alloys shifted to anodic direction with the increase of sodium hydroxide concentrations. Figure 6 compares the variation of the corrosion rate Ni–Co alloys with the increase of Co content in 0.01 M, 0.1 M and 1.0 M NaOH solutions. The corrosion rate of the electroplated Ni–Co alloys in 0.01 M NaOH solution increased gradually from 0.00193 mm/year of Ni-17.68Co to 0.135 mm/year of Ni-92.05Co. However, the corrosion rate of pure Co decreased slightly than the corrosion rate obtained for Ni-92.05Co to 0.123 mm/year.

The corrosion rate of the electroplated Ni–Co alloys in 0.1 M increased gradually from 0.00503 to 0.398 mm/year with the increase of Co content. Moreover, the corrosion rate of the electroplated Ni–Co alloys in 1.0 M NaOH solution increased more sharply with the increase of Co content. Ni showed the lowest corrosion rate in 1.0 M which accounted to be 0.0279 mm/year, while Ni-92.05Co gave the highest corrosion rate in 1.0 M NaOH which was 0.909 mm/year.

The composition and morphological structure of the electroplated Ni–Co alloys has a great effect on their electrochemical behaviour in sodium hydroxide solutions. The low corrosion rate is obtained for electroplated Ni–Co alloys with low Co%, which can be due to the formation of Ni-hydroxide, Ni-oxide and Ni-oxyhydroxides as shown in Eqs. 1–5 [21]:

$$\mathrm{Ni} + 3\mathrm{H_2O} \rightarrow \mathrm{Ni(OH)_2} \cdot \mathrm{H_2O} + 2\mathrm{H^+} + e \quad (1)$$

$$\mathrm{Ni(OH)_2} \cdot \mathrm{H_2O} + \mathrm{OH^-} \rightarrow \mathrm{NiOOH} \cdot \mathrm{H_2O_{1+x}} + (1-x)\mathrm{H_2O} + e) \quad (2)$$

or [22]:

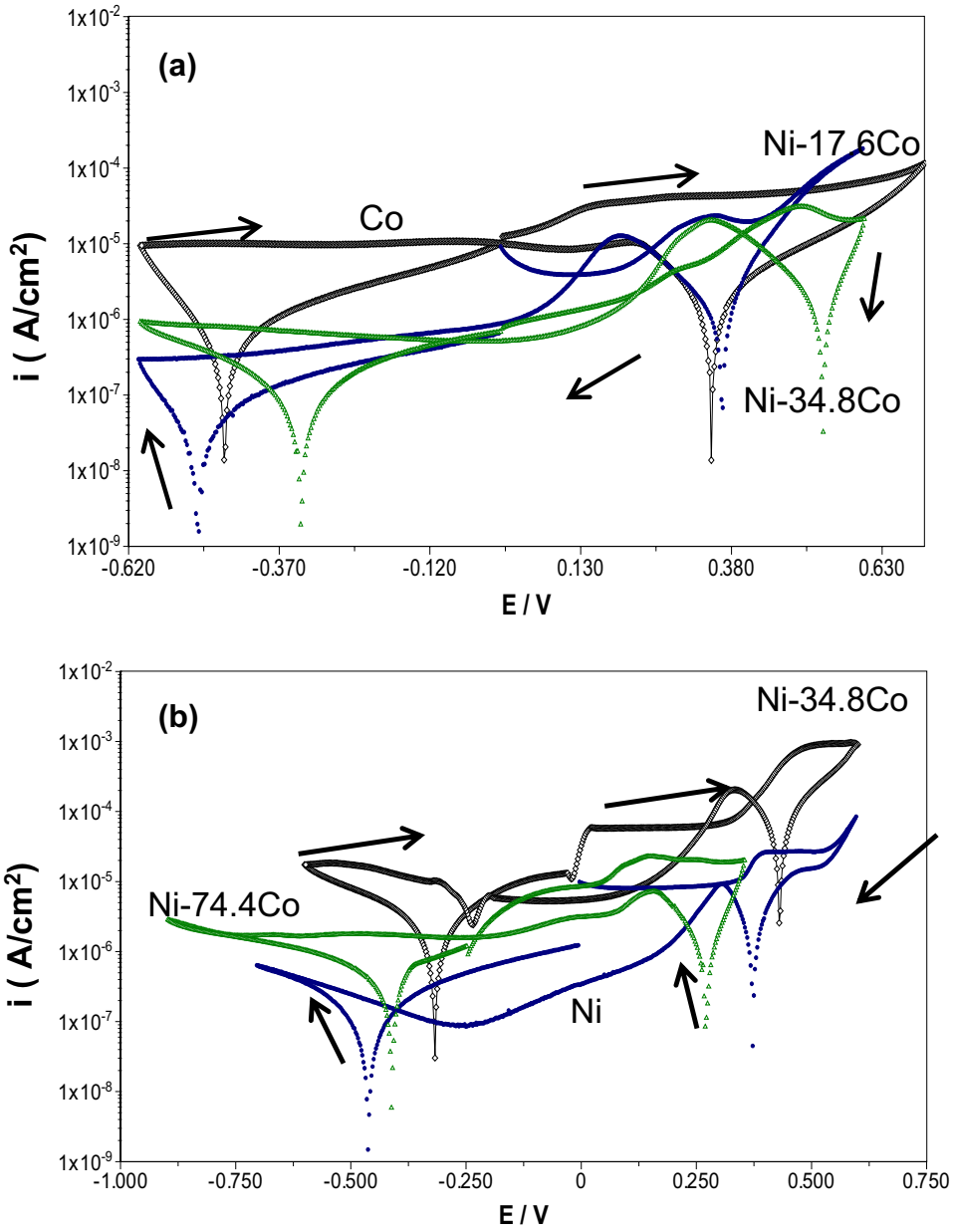

Fig. 5 Potentiodynamic polarization curves of the electroplated Ni, Co and Ni–Co alloys in NaOH solution with a scan rate of 10 mV/s; **a** for Ni-17.6Co, Ni-34.81Co and Co in 0.01 M NaOH solution; and **b** different Ni–Co alloys in 0.1 M NaOH solution

$$Ni + OH^- \rightarrow NiOH^+ + 2e \quad (3)$$

$$NiOH^+ + OH^- \rightarrow Ni(OH)_2 \quad (4)$$

$$NiOH^+ \rightarrow NiO + H^+ \quad (5)$$

From Eqs. (1) and (2), water molecules adsorb at the working electrode surface and produce Ni hydroxide, which reacts with hydroxyl ion and forms oxyhydroxide. Also, hydroxyl ions can directly react with the metal surface and produce hydroxide and oxides. The stability of the formed layers on the surface of the coatings can be affected by increasing of Co content which can accelerate the dissolution of the layer leading to increase the i_{corr} for Ni–Co alloys. Electroplated Ni and Ni–Co alloys with low Co% show generally the lowest rate of corrosion in sodium hydroxide solutions because of Ni-oxides and Ni-hydroxides. Ni-oxides and Ni-oxyhydroxides are stable which prevent continuous dissolution of Ni coating [23, 24]. However, the electroplated Ni–Co alloys with high Co% show high corrosion current densities and corrosion rate suggesting the continuous dissolution of oxyhydroxide layer. This is because cobalt is more active and susceptible to oxidation than nickel. Moreover, Tury et al. [21] revealed that the Co-based alloys produce no layer or a very thin layer, spongy oxide layer and porous CoOOH [25], causing the high dissolution rate [26]. Consequently, Co participates

Table 3 Corrosion data of Ni, Co and different Ni–Co alloys in NaOH solutions of (0.01, 0.1 and 1.0 M) at 293 K

Sample	NaOH/M	i_{corr} (μA/cm^2)	$-\beta_c$ (mV/dec)	β_a (mV/dec)	E_{corr} (V)
Ni	0.01	0.05	115	34	−0.473
	0.10	0.13	61	66	−0.460
	1.00	0.72	176	58	−0.408
Ni-17.68Co	0.01	0.08	128	85	−0.509
	0.10	1.12	75	64	−0.380
	1.00	3.35	244	98	−0.375
Ni-34.81Co	0.01	0.1	54	131	−0.340
	0.10	1.50	62	64	−0.350
	1.00	4.32	151	95	−0.370
Ni-42.44Co	0.01	0.924	192	287	−0.385
	0.10	4.98	103	98	−0.370
	1.00	8.23	87	94	−0.374
Ni-60.21Co	0.01	1.16	49	98	−0.470
	0.10	7.65	115	162	−0.403
	1.00	9.35	116	57	−0.400
Ni-74.46Co	0.01	1.17	247	66	−0.320
	0.10	8.69	367	54	−0.380
	1.00	16.3	174	89	−0.490
Ni-92.05Co	0.01	3.5	63	121	−0.487
	0.10	10.3	131	82	−0.486
	1.00	23.5	103	155	−0.472
Co	0.01	3.2	164	154	−0.470
	0.10	10	93	144	−0.480
	1.00	22.7	368	128	−0.500

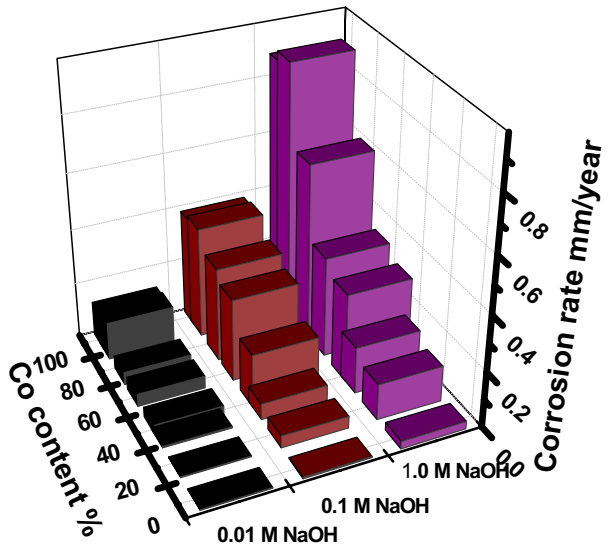

Fig. 6 Variation of corrosion rate for electroplated Ni–Co alloys with Co content in 0.01 M, 0.1 M and 1.0 M NaOH solutions at 293 K

minimal effect in the formation of the protective film [27, 28]. In addition, the morphological structure or small grains of electroplated Ni–Co alloys with low Co% is dense and smooth which can lead to the formation of dense oxide/oxyhydroxide protective layer, which decreases the corrosion rate in NaOH solution. In contrary, the electroplated Ni–Co alloys with high Co% possess granular or spherical structure which can form non-dense or porous oxide/oxyhydroxide layer decreasing the formation of the protective layer which increases the corrosion rate.

4 Conclusion

The cathodic polarization measurements indicate that the gluconate, boric acid and cysteine shift electroplating potential of Ni and Co to less negative values and decrease the overpotential of Ni and Co reduction reaction enhancing the electroplating of the Ni–Co alloys. The surface morphology of electroplated Ni–Co alloys was changed from porous to dense and coral reef-like. Nanocrystalline Ni–Co alloys are obtained as a result of the addition of sodium gluconate, boric acid and cysteine that remove pores and produce lustrous or mirror-like coatings. The increase of Co Content led to the formation of a granular structure. The electroplated Ni–Co alloys with Co% of 0–75% arranged in FCC structure but the electroplated Ni–Co alloys with Co% more than 75% possessed HCP structure. Potentiodynamic polarization showed that electroplated Ni–Co alloys with low Co% possessed lower i_{corr} and corrosion rate than electroplated Ni–Co alloys with high Co%.

Acknowledgements Authors acknowledge with thanks the financial supports granted by the Egyptian Cultural Bureau, the authors are grateful to the ACMA service at University of Newcastle, UK for SEM, XRD and EDX analysis.

Compliance with Ethical Standards

Conflict of interest The authors declare that they have no conflict of interest.

References

1. Landolt D (2002) Electrodeposition science and technology in the last quarter of the twentieth century. J Electrochem Soc 149:S9–S20
2. Orinakova R, Turonova A, Kladekova D, Galova M, Smith R (2006) Recent developments in the electrodeposition of nickel and some nickel- based alloys. J Appl Electochem 36:957–972
3. El-Feky H, Negem M, Roy S, Helal N, Baraka A (2013) Electrodeposited Ni and Ni-Co alloys using cysteine and

conventional ultrasound waves. Science China Chem 56:1446–1454
4. Hashem N, Negem M (2016) Ni-Cu nano-crystalline alloys for efficient electrochemical hydrogen production in acid water. RSC Adv 6:51111–51119
5. Nady H, Negem M (2018) Electroplated Zn–Ni nanocrystalline alloys as an efficient electrocatalyst cathode for the generation of hydrogen fuel in acid medium. Int J Hydrogen Energy 43:4942–4950
6. Negem M, Hashem N (2017) Electroplated Ni-Cu nanocrystalline alloys and their electrocatalytic activity for hydrogen generation using alkaline solutions. Int J Hydrogen Energy 42:28386–28396
7. Negem M, Nady H, El-Rabiei MM (2019) Nanocrystalline nickel–cobalt electrocatalysts to generate hydrogen using alkaline solutions as storage fuel for the renewable energy. Int J Hydrogen Energy 44:11411–11420
8. Badawy WA, Nady H, Negem M (2014) Cathodic hydrogen evolution in acidic solutions using electrodeposited nano-crystalline Ni-Co cathodes. Int J Hydrogen Energy 39:10824–10832
9. Hansal W, Tury B, Halmdienst M, Varsanyi M, Kautek W (2006) Pulse reverse plating of Ni-Co alloys: deposition kinetics of Watts, sulphamate and chloride electrolytes. Electrochim Acta 52:1145–1151
10. Davis JR (2000) Nickel, cobalt, and their alloys. Novelty, ASM International USA, p 9
11. Nady H, Negem M (2017) Microstructure and corrosion behavior of electrodeposited NiCo, NiZn and NiCu nanocrystalline coatings in Alkaline solution Z. Phys Chem 231:1159–1178
12. Mason T (1996) Advances in sonochemistry, 4th edn. JAI Press Ltd, London, p 230
13. Bhandari A, Hearne S, Sheldon B, Soni S (2009) Microstructural origins of saccharin-induced stress reduction in electrodeposited Ni. J Electrochem Soc 156:D279–D282
14. Tian L, Xu J, Qiang C (2011) The electrodeposition behaviors and magnetic properties of Ni–Co films. Appl Surf Sci 257:4689–4694
15. Zech N, Landolt D (2000) The influence of boric acid and sulfate ions on the hydrogen formation in Ni-Fe plating electrolytes. Electrochim Acta 45:3461–3471
16. Hoare JP (1986) On the role of boric acid in the Watts Bath. J Electrochem Soc 133:2491
17. Oniciu L, Muresan L (1991) Some fundamental aspects of levelling and brightening in metal electrodeposition. J Appl Electrochem 21:565–574
18. Wu BYC (2002) Synthesis and characterization of nanocrystalline alloys in the binary Ni–Co system. M.Sc. Thesis University of Toronto
19. Tury B, Lakatos-Varsányi M, Roy S (2006) Ni–Co alloys plated by pulse currents. Surf Coat Technol 200:6713–6717
20. Klung H, Alexander L (1974) X-ray diffraction procedures for polycrystalline and amorphous materials. Wiley, New York, p 618
21. Tury B, Lakatos-Varsanyi M, Roy S (2007) Effect of pulse parameters on the passive layer formation on pulse plated Ni–Co alloys. Appl Surf Sci 253:3103–3108
22. Sato N, Okamoto G (1963) Anodic passivation of nickel in sulfuric acid solutions. J Electrochem Soc 110:605
23. Kang J, Yang Y, Shao H (2009) Comparing the anodic reactions of Ni and Ni–P amorphous alloy in alkaline solution. Corr Sci 51:1907–1913
24. Komath M (1996) Hot corrosion of nickel in anhydrous sodium hydroxide. Mater Chem Phys 45:171–175
25. Casella IG, Guascito MR (1999) Anodic electrodeposition of conducting cobalt oxyhydroxide films on a gold surface. XPS study and electrochemical behaviour in neutral and alkaline solution. J Electroanal Chem 476:54–63
26. Kim S, Tryk DA, Antonio MR, Carr R, Scherson D (1994) In situ x-ray absorption fine structure studies of foreign metal ions in nickel hydrous oxide electrodes in alkaline electrolytes. J Phys Chem 98:10269–10276
27. Bo Y, Hwang E, Scherson DA (1996) In situ quartz crystal microbalance studies of nickel hydrous oxide films in alkaline electrolytes. J Electrochem Soc 143:37
28. Zhao H, Liu L, Zhu J, Tang Y, Hu W (2007) Microstructure and corrosion behavior of electrodeposited nickel prepared from a sulphamate bath. Mater Lett 61:1605–1608